

Electronic Supplementary Information (ESI) for: Near-equilibrium measurement of quantum size effects using Kelvin probe force microscopy

Thomas Späth,^{†,‡} Matthias Popp,[†] Carmen Pérez León,^{*,†} Michael Marz,[†] and
Regina Hoffmann-Vogel^{†,¶}

Karlsruhe Institute of Technology (KIT), 76128 Karlsruhe, Germany

E-mail: carmen.perez.leon@kit.edu

Contents:

- I- Simple model for calculating the Fermi energy
- II- Additional experimental details on Pb deposition
- III- Atomically resolved SFM image of a Pb island. Figure S1
- IV- Statistical averaging methods. Figures S2, S3, S4
- V- Extra data at large island heights. Figure S5
- VI- Fitting parameters. Table S1

*To whom correspondence should be addressed

[†]Physikalisches Institut, Karlsruhe Institute of Technology (KIT), 76128 Karlsruhe, Germany

[‡]Current address: Department of Materials Science, Darmstadt University of Technology, 64287 Darmstadt, Germany

[¶]Institut für Angewandte Physik, Karlsruhe Institute of Technology (KIT), 76128 Karlsruhe, Germany

I - Simple model for calculating the Fermi energy

In this section, we will calculate the Fermi energy for thin films. The electrons in the Pb islands can move almost freely in the lateral direction in the island. In the direction perpendicular to the surface, the electrons are confined in the potential well formed between the vacuum-metal interface on one side and the band gap of the Si surface (the substrate) at the other side resulting in the quantization of the energy levels¹. Thus, the number of states in x - and y -direction is quasi-continuous whereas in the z -direction the wavevector component k_z is quantized. Consequently, the Fermi sphere of allowed states is reduced to a discrete number of Fermi discs with a constant k_z value.

We will use the solution of the Schrödinger's equation for a potential well with a thickness a and a lateral extension of L , where $L \gg a$. The wavefunction is separable into three parts for the three spatial directions:

$$\Psi(x, y, z) = \Psi_1(x)\Psi_2(y)\Psi_3(z), \quad (\text{S1})$$

The solution in x - and y -direction are plane waves, whereas in z -direction, this is given by the solution of the one-dimensional Schrödinger's equation for the potential barrier of the well.

The number of available electronic states is determined by the area of the Fermi discs (Figure 1a). The state with $k_z = 0$, i.e. $n_z = 0$, is a non-physical solution of the equation. The state with k_z is equal to the state $-k_z$ and is therefore not counted, only $n_z > 0$ values are valid. For $n_z = 1$, the area is given by:

$$A_1 = \pi(k_F^2 - k_{z,1}^2) \quad (\text{S2})$$

and the number of states by:

$$N_1 = \left(\frac{L}{2\pi}\right)^2 \cdot \pi(k_F^2 - k_{z,1}^2). \quad (\text{S3})$$

For an arbitrary ℓ , being $\ell < n_z$ and $2n_z$ the number of available Fermi discs, the number of available states is then given by:

$$N_{n_z} = \left(\frac{L}{2\pi}\right)^2 \cdot \pi \sum_{\ell=1}^{n_z} (k_F^2 - k_{z,\ell}^2). \quad (\text{S4})$$

Not to forget that the total number of states is twice as large due to the two possible spin orientations, thus

$$N = 2 \cdot N_{n_z}. \quad (\text{S5})$$

On the other hand, the number of electrons in the island is $N = \rho V = \rho L^2 a$, ρ being the electron density. Resolving for the Fermi wavevector k_F , we obtain:

$$k_F = \sqrt{\frac{2\pi\rho a + \sum_{\ell=1}^{n_z} k_{z,\ell}^2}{n_z}}, \quad (\text{S6})$$

and for the Fermi energy:

$$E_F = \frac{\hbar^2}{2m} \frac{2\pi\rho a + \sum_{\ell=1}^{n_z} k_{z,\ell}^2}{n_z}. \quad (\text{S7})$$

Both Equations S6 and S7 describe a set of curves for varying n_z . The Fermi energy of the island is thus piecewise defined by the state that has the lowest energy for a given island thickness.

I.1 Infinite potential well:

Using the boundary conditions of an infinite potential well, the wavefunctions must be zero at the borders of the well:

$$k_z \cdot a = n_z \pi \quad \rightarrow \quad a = n_z \cdot \frac{1}{2} \lambda_z, \quad (\text{S8})$$

where n_z is an integer. Consequently, the island's thickness a must be a multiple of the half of the wavelength λ_z . In the k_z -direction, the distance between states, π/a , decreases by

increasing the thickness of the island a .

Using Equation S8, $k_z = n_z\pi/a$, with a distance between states of π/a , Equation S4 can be simplified to

$$N_{n_z} = \left(\frac{L}{2\pi}\right)^2 \cdot \pi \sum_{\ell=1}^{n_z} (k_F^2 - k_{z,\ell}^2) = \left(\frac{L}{2\pi}\right)^2 \cdot \left(\pi n_z k_F^2 - \pi \left(\frac{\pi}{a}\right)^2 \sum_{\ell=1}^{n_z} \ell^2 \right). \quad (\text{S9})$$

The sum is equal to

$$\sum_{\ell=1}^{n_z} \ell^2 = \frac{1}{6} n_z (n_z + 1) (2n_z + 1), \quad (\text{S10})$$

such that

$$k_F = \sqrt{\frac{2\pi\rho a}{n_z} + \frac{\pi^2}{6} \frac{(n_z + 1)(2n_z + 1)}{a^2}}. \quad (\text{S11})$$

The value of k_F decreases for small a proportional to $1/a$, has a minimum and increases again for large a proportional to \sqrt{a} .

We now write the sample thickness a as a function of the bulk Fermi wavelength $\lambda_{F,bulk}$ as $a = r\lambda_{F,bulk}$, where $r = n_z/2$. In addition, we divide k_F by its bulk value and get:

$$\frac{k_F}{k_{F,bulk}} = \sqrt{\frac{4}{3} \frac{r}{n_z} + \frac{1}{24} \frac{(n_z + 1)(2n_z + 1)}{r^2}}, \quad (\text{S12})$$

that is ρ independent. Using that $E_F = (\hbar k_F)^2/(2m)$, we obtain for the Fermi energy:

$$\frac{E_F}{E_{F,bulk}} = \frac{k_F^2}{k_{F,bulk}^2} = \frac{4}{3} \frac{r}{n_z} + \frac{1}{24} \frac{(n_z + 1)(2n_z + 1)}{r^2}. \quad (\text{S13})$$

These equations, as in the case of k_F and E_F in Equations S6 and S7, describe a set of curves for varying n_z . The Fermi energy of the island is piecewise defined by the state that has the lowest energy for a given island thickness. The points where the curves intersect occur roughly at the integer multiples of $\lambda_{F,bulk}/2$. For large n_z , the minima of the curves converges versus the bulk value $E_{F,bulk}$. However, the ratio $E_F/E_{F,bulk}$ decays rather than oscillates and does not reproduce our experimental results.

I.2 Finite potential well:

Using instead a finite potential well, the wavefunction can leak out of the potential well, and k_z can be arbitrarily small as long as the potential barrier of the well also remain small. Inside the well, the wavefunction is described by a sinusoidal function, whereas outside the well it is described by an exponential decaying wavefunction, with the decay exponent κ . At the borders of the well, the two functions must be differentiable. This is achieved by

$$\kappa = k_{z,n_z} \tan\left(\frac{k_{z,n_z}L}{2}\right) \quad (\text{S14})$$

for symmetric solutions, where y is similar to a cosine and by

$$\kappa = -k_{z,n_z} \cot\left(\frac{k_{z,n_z}L}{2}\right) \quad (\text{S15})$$

for asymmetric solutions, where y is similar to a sine. In addition we have

$$\kappa^2 + k_{z,n_z}^2 = \frac{2mV_0}{\hbar^2}, \quad (\text{S16})$$

where V_0 is the potential barrier of the well. k_{z,n_z} is calculated numerically with these equations. The result for $E_F/E_{F,bulk}$ is the piecewise defined curve shown in Figure 1b of the main manuscript. This graph shows the resulting Fermi energy for the different states defined by different n_z . The main features such as a dampen oscillatory behavior and an oscillation wavelength of $\lambda_{F,bulk}/2$ are well described by this model. The decay, however, is given by $1/r^2$, see Equation S13 instead of $1/r$ which is closer to our experimental observations. Although the basic physics can be understood from the considerations made here, the result does not describe the experimental data in detail.

II - Additional experimental details on Pb deposition

With the purpose of producing a large distribution of island heights, deposition parameters such as the temperature of the substrate during deposition, the evaporation flux, the deposition time, and the annealing of the sample after deposition were varied. In addition, the aperture of the crucible was opened and closed during deposition for obtaining a coverage gradient on the surface, but this procedure turned out to produce only a weak effect. The shutter was slowly opened manually during 5 s and then closed again during the following 5 s, and this procedure was repeated for the entire evaporation process. Prior to Pb evaporation, for some samples the Si(111) substrate was cooled down to room temperature, whereas for other samples the Si substrate was first cooled to liquid nitrogen temperature and then annealed at room temperature for times between 20 and 40 min. The Pb (99.9995% purity, Balzers) was evaporated from a crucible with a Mini e-Beam evaporator containing four pockets and a EGCO4 power supply (Oxford Applied Research). The evaporation flux and time were adjusted between 10 – 50 nA and 20 – 50 s to obtain an averaged Pb layer thickness of a few nanometers. After Pb deposition, the samples were transferred immediately to the liquid nitrogen pre-cooled scanning force microscope (Omicron VT-AFM) at ~ 110 K attached to the same vacuum vessel for the scanning force microscopy measurements.

III - Atomically resolved SFM image on a Pb island

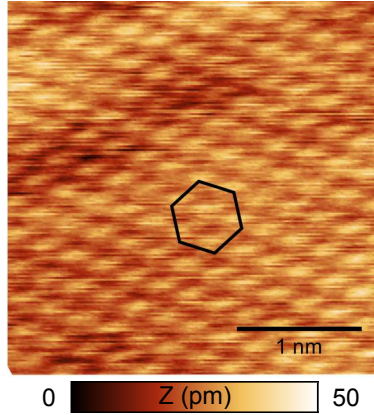


Figure S1: Atomically resolved SFM topographic image obtained in the dynamic mode with FM detection. Flat-top mesa shaped (111)-oriented Pb islands grow on Si(111) surrounded by a wetting layer. The black hexagon highlights the atomic arrangement of the Pb(111) surface. The image has been drift-corrected.

Imaging parameters: $(3 \times 3) \text{ nm}^2$; $\Delta f = -57 \text{ Hz}$, $A = 8 \text{ nm}$, $k = 50 \text{ N/m}$, $f_0 = 280059 \text{ Hz}$, $\gamma = -7.3 \text{ fN}\sqrt{\text{m}}$. Pt-Ir coated tip.

IV - Statistical averaging methods

Our SFM images in Figure 2 of the main manuscript show small Pb islands, several of them partly extending over more than one Si(111) terrace or having internal height differences. We analyzed the islands using a statistical averaging method that we introduce in the following for a Pb island having one particular height, and, accordingly, one defined local work function (LWF). This method has been proven to be suitable also for islands spreading over several Si terraces. First, the image of a single Pb island was cut from an overview image (as shown in Figure S2a). A histogram of the measured heights was generated for the cut image (see Figure S2b,c). Figure S2a is the same image as Figure 2a, but leveled such that the terraces and the island's surfaces are horizontally flat. This leveling is useful for the analysis with histograms. The peak in the histogram corresponding to the height of the island and the peak corresponding to the height of the terrace where the island sits were identified and

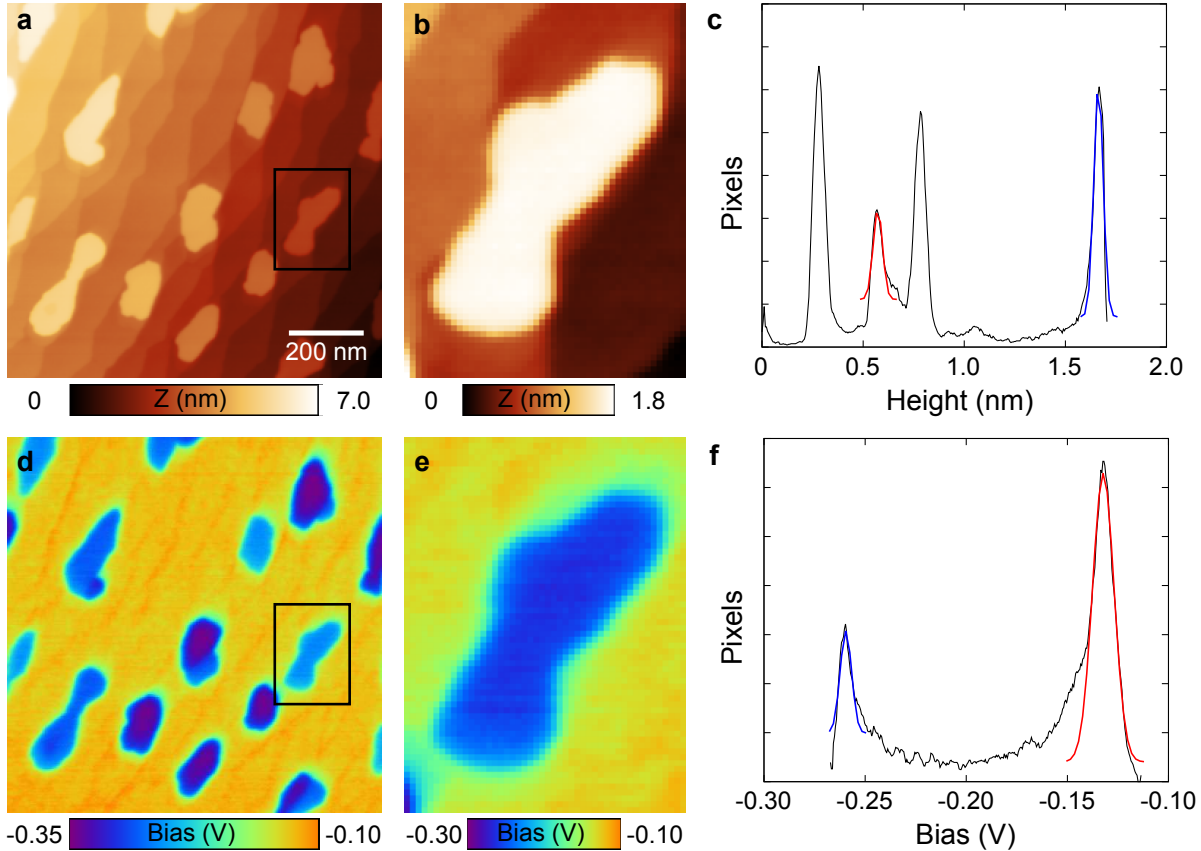


Figure S2: a) Overview SFM image of small Pb islands. b) First, the image of a single island was cut. c) Then a histogram of the measured heights of the cut image was generated. The peaks corresponding to the island surface and to the terrace where the island sits were identified and fitted by Gaussian functions (in blue and red respectively). The terraces are covered by the wetting layer. A similar procedure was applied to the Kelvin image: d) Overview Kelvin image of Pb islands, e) cut image of an island, and f) corresponding histogram generated from e.

fitted by a Gaussian function, blue and red fits respectively. This height corresponds to the height of the terrace covered by the wetting layer (WL). Since, as we explained in the main manuscript our strategy is to analyze the data using the WL as reference, the difference between the two centers of the Gaussian functions was taken to be the island height. The same procedure was performed for the Kelvin images (Figure S2d–f). In this way the LWF values are referred to the WL, and we obtain tip-independent results.

Figure S3 shows the data results after the statistical analysis of many experiments performed with one single Pt/Ir-coated tip. The height of the islands with respect to the WL is

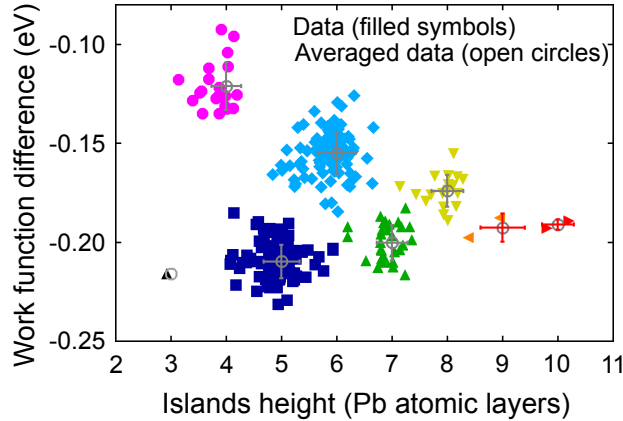


Figure S3: Data results after the statistical analysis of many experiments performed with one single Pt/Ir-coated tip. They correspond to the statistical spread of the data in Figure 4 of the main manuscript (here shown in grey). Different island heights and distinct local work function differences are clearly identified. The local height of the islands is given in atomic layers measured from the WL.

given in Pb atomic layers. In the graph, the data resulting from a particular island thickness can be easily identified. For every height, the data were averaged and plotted with error bars (in grey in Figure S3). These averaged results correspond to the data in Figure 4 of the main manuscript.

The results obtained from different several measurement series using different tips are shown in Figure S4. It is noticeable that data obtained with different tips align well with each other, confirming that we indeed obtain tip-independent results.

V - Extra data at large island heights

In addition to the data shown in the main paper, we have studied thicker islands. As was discussed in the main text, the amplitude of the bilayer oscillation of the LWF with respect to the film thickness decays with for increasing island height. The oscillation is additionally modulated by a quantum beating pattern that causes a periodical phase slip every nine to ten atomic layers. This implies an increase of the oscillation amplitude for islands higher than the investigated range in the main manuscript (10 atomic layers). The purpose of this

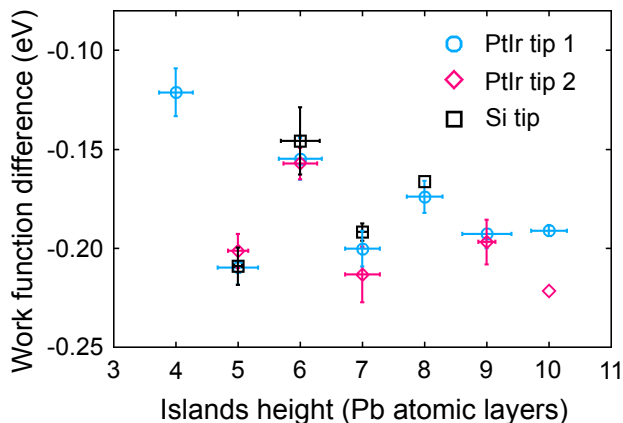


Figure S4: Quantum oscillations in the local work function of ultra-thin Pb islands on Si(111) as a function of the island height measured from the WL obtained with diverse tips. The averaged data with error bars are plotted. Data obtained with different tips align well with each other, proving that we indeed obtain tip-independent results.

study is to confirm the existence of a beating pattern and to precisely locate the island height for which the knot of the quantum beating pattern is observed.

Large island heights were obtained by annealing the samples at room temperature after lead evaporation for a defined time (between 15 and 90 min). Subsequently, the sample was cooled down with liquid nitrogen for SFM measurements. Afterwards, the samples were repeatedly warmed up and cooled down again for further measurements. The results of this new set of experiments with combined SFM and Kelvin probe force microscopy (KPFM) were analyzed using different methods than for the case of lower island heights. In this case, line profiles over the images were used to determine the island heights and their Kelvin voltage. The values obtained for the thinner islands or part of the islands below 10 atomic layers in height measured from the WL mostly agree with the data shown in Figure 4 of the main manuscript. Figure S5 presents the additional data for islands up to 14 atomic layers measured from the WL combined with the results of Figure 4. An increase of the quantum oscillation amplitude and a reversal of maxima and minima beyond 10 atomic layers is clearly observed, the knot being placed between 9 – 10 atomic layers from the WL.

We observe that the value of the LWF difference obtained on some samples of this additional set of experiments for obtaining higher islands is shifted by few mV towards more

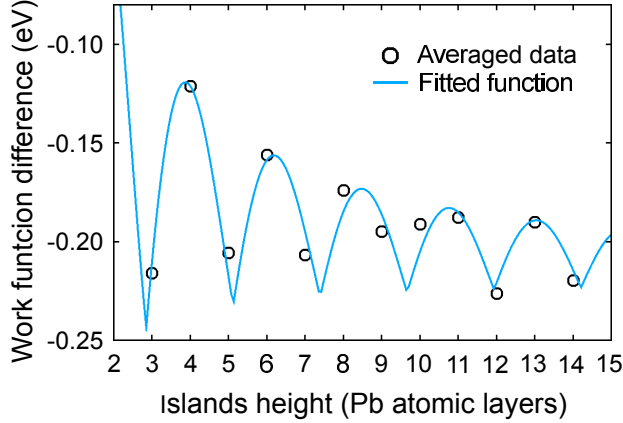


Figure S5: Quantum oscillations in the local work function of Pb islands on Si(111) with island heights up to 14 atomic layers as a function of the island height measured from the WL obtained with SFM/KPFM. Results obtained from an additional set of experiments including data at larger island heights combined with the data from Figure 4 of the main manuscript. In addition to the damped even-odd oscillating with increasing island height, these data show the quantum beating pattern: At nine atomic layers the amplitude of the oscillation vanishes and increases again for larger film thicknesses. Data fitted with function of Equation 6 of the main manuscript and Equation S17 of Supporting Information ($\alpha = 1.02$).

negative values with respect to the other samples and to results in Figure 4 of the main manuscript. These shifts appear for samples that have been exposed to long annealing times at room temperatures (at least 90 min). We also observed that if the samples were kept long enough at low temperatures (several days), the LWF shifted back to the original values. It is important to state that these shifts affect a particular measurement series as a whole, and not only data for particular islands' heights. Here, we are interested in the decay of the oscillation amplitude as a function of the film thickness, and in the position of the knot of the beating pattern, i.e. the phase of the beating pattern. Thus, we have chosen only similar data for averaging, ensuring that the amplitude of the oscillation is not markedly influenced by the shifts.

We tentatively explain the shifts of the LWF differences to be due to variations in the LWF of our reference, the wetting layer. The WL is a dynamic system that transfers material collectively to islands even at low temperatures.² This material comes from unstable islands and the WL itself.²⁻⁴ The thickness of the WL was reported to be between 1 – 3 atomic layers

depending on the growth temperature,^{3,5} but it is now generally agreed that it is around one atomic layer.^{6,7} The density of the WL is 22% larger than the metallic Pb(111) density.⁴ This is possible because the Si substrate facilitates the Pb atoms to move closer than their average distance in bulk Pb.⁴ It has been pointed out that fluctuations exist within the WL, suggesting variations in the WL density.⁸ We presume that the long annealing at room temperature for obtaining large islands affects the structure of the WL. Due to coarsening, the WL rearranges or loses atoms that are transferred to larger islands. This possibly has as consequence a decrease in density of the WL. This less dense WL would have a higher LWF than the usual dense one, and the LWF difference between the islands and the WL would be larger, i.e. more negative, like the shift that we observe in our samples annealed for long times.

VI - Fiting parameters

The phenomenological damped sinusoidal function reported in the main manuscript as Equation 6:

$$f(N) = \frac{A|\sin Nk_F d_0 + \phi| + B}{N^\alpha} + C, \quad (\text{S17})$$

has been used to describe the periodicity and decay of the oscillation of the LWF as a function of the number of atomic layers measured from the WL (N), as well as the beating pattern. In Equation S17, A (amplitude parameter), B (amplitude offset), C (constant offset), ϕ (phase shift factor that will be dependent on the interface properties of the film), and α (the decay exponent) are N -independent constants,^{9,10} and k_F is the Fermi wave vector measured from the zone boundary (see explanation below).¹¹

To evaluate the decay exponent of the oscillations, we have fitted this equation to our data of Figure 4 and Figure S5. The values obtained for the free parameters are presented in Table S1. The value of α is larger than 1 for the fit of the data in Figure 4 due to the fitting only up to the first beating pattern. If we use data up to 14 atomic layers, the value

Table S1: Free parameters obtained after fitting the experimental data with the damped sinusoidal function given in Equation 6 of the main manuscript, here Equation S17.

	Fig. 4	Fig. S5
A	0.595 ± 0.200 eV	0.473 ± 0.235 eV
B	-0.06 ± 0.08 eV	-0.07 ± 0.09 eV
C	-0.210 ± 0.010 eV	-0.218 ± 0.010 eV
α	1.26 ± 0.20	1.02 ± 0.30
φ	2.62 ± 0.03	2.35 ± 0.06

gets closer to the expected $\alpha = 1$.

Using λ_F and d_0 given in the main text for free electrons, we obtain $k_F d_0 = 1.44\pi$. With these values, Equation S17 has a period of less than one atomic layer and cannot be observed experimentally due to the discrete nature of the atomic layer structure of the films. The number of oscillations of the fit function is better described by the Fermi wave vector measured from the zone boundary, here $k_F d_0 = 0.44\pi$ and the oscillation period is around 2.

References

- (1) Milun, M.; Pervan, P.; Woodruff, D. P. *Rep. Prog. Phys.* **2002**, *65*, 99–141.
- (2) Man, K. L.; Tringides, M. C.; Loy, M. M. T.; Altman, M. S. *Phys. Rev. Lett.* **2008**, *101*, 226102.
- (3) Hupalo, M.; Kremmer, S.; Yeh, V.; Berbil-Bautista, L.; Abram, E.; Tringides, M. C. *Surf. Sci.* **2001**, *493*, 526–538.
- (4) Hershberger, M. T.; Hupalo, M.; Thiel, P. A.; Wang, C. Z.; Ho, K. M.; Tringides, M. C. *Phys. Rev. Lett.* **2014**, *113*, 236101.

- (5) Qi, Y.; Ma, X.; Jiang, P.; Ji, S. H.; Fu, Y. S.; Jia, J. F.; Xue, Q. K.; Zhang, S. B. *Appl. Phys. Lett.* **2007**, *90*, 013109.
- (6) Wang, L.; Ma, X. C.; Jiang, P.; Fu, Y. S.; Ji, S. H.; Jia, J. F.; Xue, Q. K. *J. Phys.: Cond. Matter* **2007**, *19*, 306002.
- (7) Kim, J.; Zhang, C.; Kim, J.; Gao, H.; Chou, M.-Y.; Shih, C.-K. *Phys. Rev. B* **2013**, *87*, 245432.
- (8) Hattab, H.; Hupaló, M.; Hershberger, M. T.; von Hoegen, M. H.; Tringides, M. C. *Surf. Sci.* **2016**, *646*, 50–55.
- (9) Wei, C. M.; Chou, M. Y. *Phys. Rev. B* **2002**, *66*, 233408.
- (10) Czoschke, P.; Hong, H.; Basile, L.; Chiang, T.-C. *Phys. Rev. B* **2005**, *72*, 075402.
- (11) Miller, T.; Chou, M. Y.; Chiang, T.-C. *Phys. Rev. Lett.* **2009**, *102*, 236803.